# The compositions of rock-forming and accessory minerals from the Gemeric granites (Hnilec area, Gemeric Superunit, Western Carpathians)

*IGOR BROSKA[1] – MICHAL KUBIŠ[1] – C. TERRY WILLIAMS[2] – PATRIK KONEČNÝ[3]*

[1]Geological Institute, Slovak Academy of Sciences, Dúbravská cesta 9, 842 26 Bratislava, Slovakia; e-mail: geolbros@savba.sk
[2]Department of Mineralogy, The Natural History Museum, Cromwell Road, London, SW7 5BD, United Kingdom
[3]Geological Survey of Slovak Republic, Mlynská dolina 1, 817 04 Bratislava, Slovakia

Abstract. The Hnilec granites represent a suite of specialized S-type granite massifs in the Western Carpathians, with a primary enrichment in elements B, F, Sn, Nb, Ta and W being reflected in a suite of characteristic minerals (e.g. tourmaline, cassiterite, and Nb-Ta phases). The highly evolved nature of these granites results from a lowering of the viscosity of the primary melt, which is due to the high content of the volatiles (B, F), and an increased activity of P. Phosphorus is incorporated into primary apatite as well as in the K-feldspar, whereas the Na-feldspar (albite) is P-bearing only in the exsolved perthitic part of the K-feldspar. The majority of the perthitic albite crystals contain abundant exsolved apatite grains that in general, do not exceed 3–5 μm in size and due to the apatite exsolution, albite is low in P. Compositionally, secondary apatite in albite differs from the primary one in having low concentrations of Mn, Fe and REE. The LREE are predominantly hosted in apatite, and to a lesser extent monazite, whereas the HREE are mainly distributed in zircon, xenotime and apatite. The morphology of zircon crystals is similar in all the granitic rock types investigated, i.e. in the deep-seated coarse-grained granites, upper fine-grained granites and the greisenized cupola. Cathodoluminesce images of zircon crystals show a strong primary magmatic zonation and some secondary alteration features. These aspects of zircon morphology and composition suggest that zircon crystallized mainly in the deep magma chamber and was incorporated within the ascending differentiated melt. Some of the zircons can be classified as $G_1$ and L subtypes which represents a late magmatic population of zircon. The contribution of the early magmatic zircon to the bulk rock HREE distribution is considered to be significant. The co-magmatic features of the granites are evident from extreme differentiation leading to the zonality of the plutons and alteration of the granite, i.e. albitization and greisenization, by fluids in the cupola.

Key words: granite, two-mica granite, rock-forming minerals, accessory minerals, chemical composition, zircon, boron, fluorine, niobium, phosphorus, tantalum, tin, greisenization, albitization,Western Carpathians

## Introduction

The results of tin prospecting of the Hnilec granite during the 1970's discovered the existence of a high temperature mineralization within these granites that had intruded into the low-grade metasediments and metavolcanics. Underground mining activity has revealed the presence of zonation within the Hnilec granite body, and provided an opportunity to study its differentiation and alteration processes, including the greisens, that had occurred in the apical parts of the granite.

The S-type character of Hnilec granites is demonstrated by several features including the high initial $^{87}Sr/^{86}Sr$ ratio of 0.7119 (Cambel et al. 1990). The REE normalized pattern of the granites has a significant negative Eu anomaly (Eu/Eu* ≈ 0.02), and the Rb content ranges from 170 to 870 ppm depending on the differentiation level (Broska and Uher 2001). A high content of Fe and Al in biotite is typical along with increasing contents of Sn in biotite and low contents of MgO (3–4 wt%) and $TiO_2$ (2.5–3 wt%). On the basis a study of garnets, Faryad and Dianiška (1989) suggested the Hnilec granites originated at a depth >21 km and pressure ~850 MPa and that magma solidification occurred at a depth between 5–7 km. Zircon dating indicates a Permian/Triassic age for the Hnilec granites (243 ±18 Ma; Poller et al. 2002). A Permian age was also obtained from electron microprobe dates of monazite (276 ±13 Ma; Finger and Broska 1999), as well as an older

Rb/Sr data age (282 ±2 Ma; Cambel et al. 1990), although the contact aureole of Súľová granite (Hnilec area) has a 140 Ma date obtained by $^{40}Ar/^{39}Ar$ dating (Vozárová et al. 2000).

The Hnilec granites are characterized by their tourmaline mineralization. Tourmaline contents generally increase towards the top of the granite body. One borehole in the Hnilec granite body showed that whereas only 8 g/t of tourmaline is present at a depth of 900 m, 700 g/t occurs at 600 m, and 4200 g/t at 300 m (Rub et al. 1977). In contrast, zircon, monazite, anatase and apatite decrease in abundance with depth. The distribution of tourmaline is probably associated with its polystage development: the older magmatic tourmaline is relatively unstable, especially in the two-mica granites, and is substituted by younger, X-site deficient tourmaline, of schorl-foitite composition (Broska et al. 1998, 1999).

The western Hnilec granite occurrence called "Súľová" (Fig. 1) is a relatively large body approximately 2 x 1 km in surface area, and with a strong vertical zonal structure. The lower part is comprised of two-mica granite, the middle section consists of a medium-grained Ms granite, and the highest part is fine-grained greisenized granite. The greisen occurs in the apical endocontact parts and form 100–200 m long bodies, 30 m in height (locally even more) in vertical cross section (Fig. 2). Greisenization produced a zonal arrangement of various types of metasomatites: 1) Quartz zone (0.2–1.0 m), 2) a zone of
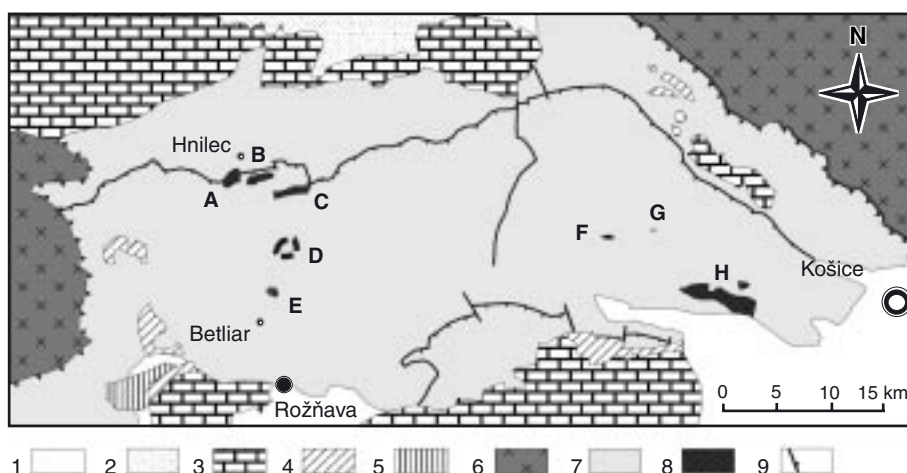
1 ☐ 2 ☐ 3 ☐ 4 ☐ 5 ☐ 6 ☐ 7 ☐ 8 ☐ 9 ☐

Fig. 1. Geological sketch map of the Spiš-Gemer granite occurrences.
Explanation: 1 – Neogene to Quaternary sedimentary rocks, 2 – Sediments of the Inner Carpathian Pale-
ogene: sandstones, claystones, 3 – Silicium: limestones, dolomites (Lower Triassic-Upper Jurassic), 4 –
Meliaticum: limestones, dark shales, radiolarites, glaucophanites (Upper Permian-Upper Jurassic), 5 –
Turnaicum: limestones, dark shales (Upper Permian-Middle Jurassic), 6 – Veporicum: paragneisses, gran-
ites, migmatites (Paleozoic), 7 – Gemericum: phyllites, metasandstones, metavolcanics (Paleozoicum), 8
– Gemeric granites, 9 – Thrust faults, A - Súľová body, B - Delava body, C - Surovec body, D - Podsúľová
body – hidden granite, E - Betliar body, F - Hummel body, G - Zlatá Idka body, H - Poproč body. The
Súľová, Delava and Surovec bodies form the Hnilec granite.

new perspective to aspects of the development of Hnilec granites, based mainly on the compositions of the feldspar and REE accessory minerals, and zircon morphology of the principal rock types of this intrusion, and compared with mineralogical and geological reviews from this region. The samples were collected from the mine dumps, and represent the typical rock types present, including greisens.

## Methodology

The samples were investigated from both thin sections and liberated accessory mineral concentrates. The heavy mineral fractions were obtained using standard mineral separation procedures, i.e. a combination of rock crushing, sieving, prelimi-

quartz-mica greisen, 3) a zone of albitized fine-grained granite together with lenses of ore greisens, 4) a zone of microclinized medium-grained granite (Grecula 1985). Tin is the main ore element in the gradual facial zones and it increases in concentration towards the contact. The disseminated Sn-W-(Li-Nb-Ta) mineralization is concentrated mainly in the greisenized cupola, quartz-cassiterite veins, as well as in the albite-Li-mica-topaz granites (Drnzík 1982).

The main scientific goal of this study is to provide a

nary concentration using a Wilfley table, and final heavy liquid and magnetic separation. The zircon morphology was studied using a binocular microscope. The cathodoluminiscence images of zircons were obtained on a Cameca SX100 (ŠGÚDŠ Bratislava) electron microprobe, as were analyses of feldspar, mica and zircon employing a variety of natural minerals and synthetic compounds as standards. Analytical parameters were an accelerating voltage of 15 kV, beam current of 20 nA, and beam diameter of 5 μm. For analyses of feldspar, a peak count time of 20 sec on each element was



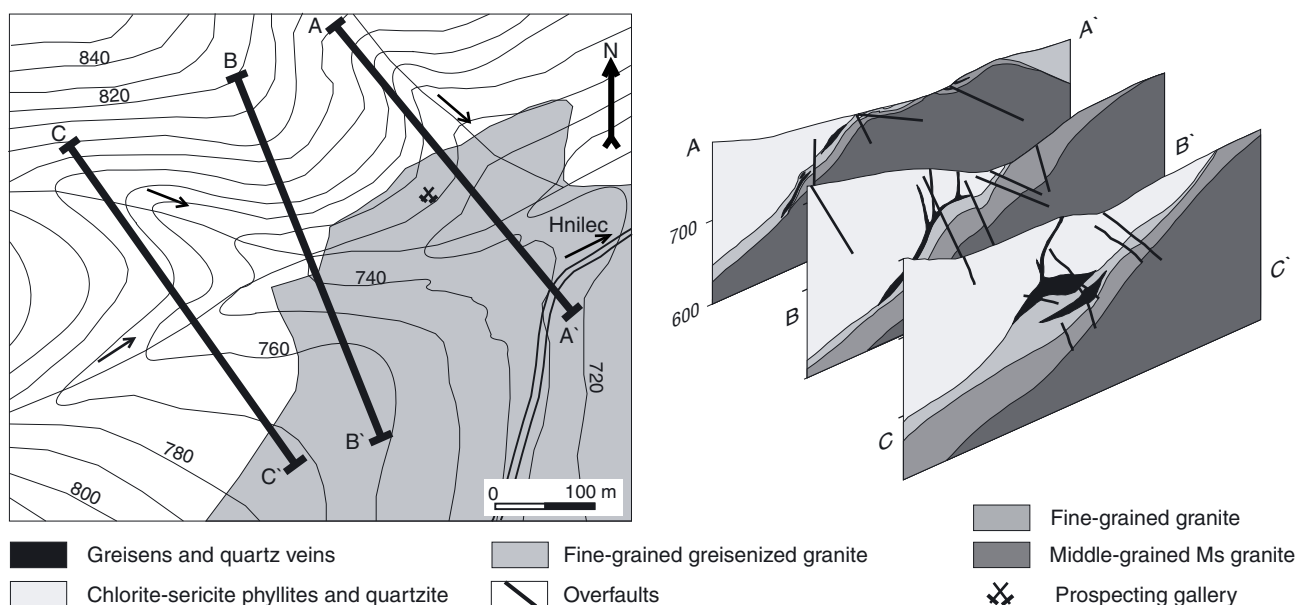| Greisens and quartz veins | Fine-grained greisenized granite | Fine-grained granite |
| Chlorite-sericite phyllites and quartzite | Overfaults | Middle-grained Ms granite |
| | | Prospecting gallery |

Fig. 2. Cross-sections of the Hnilec granite body according to mining work (Drnzík et al. 1982). Sample GK-8 was taken from the medium-grained, and GK-9 from fine-grained granite. Sample GK-10 represents the greisenized part of fine-grained granite. The granites from the map are undistinguished.
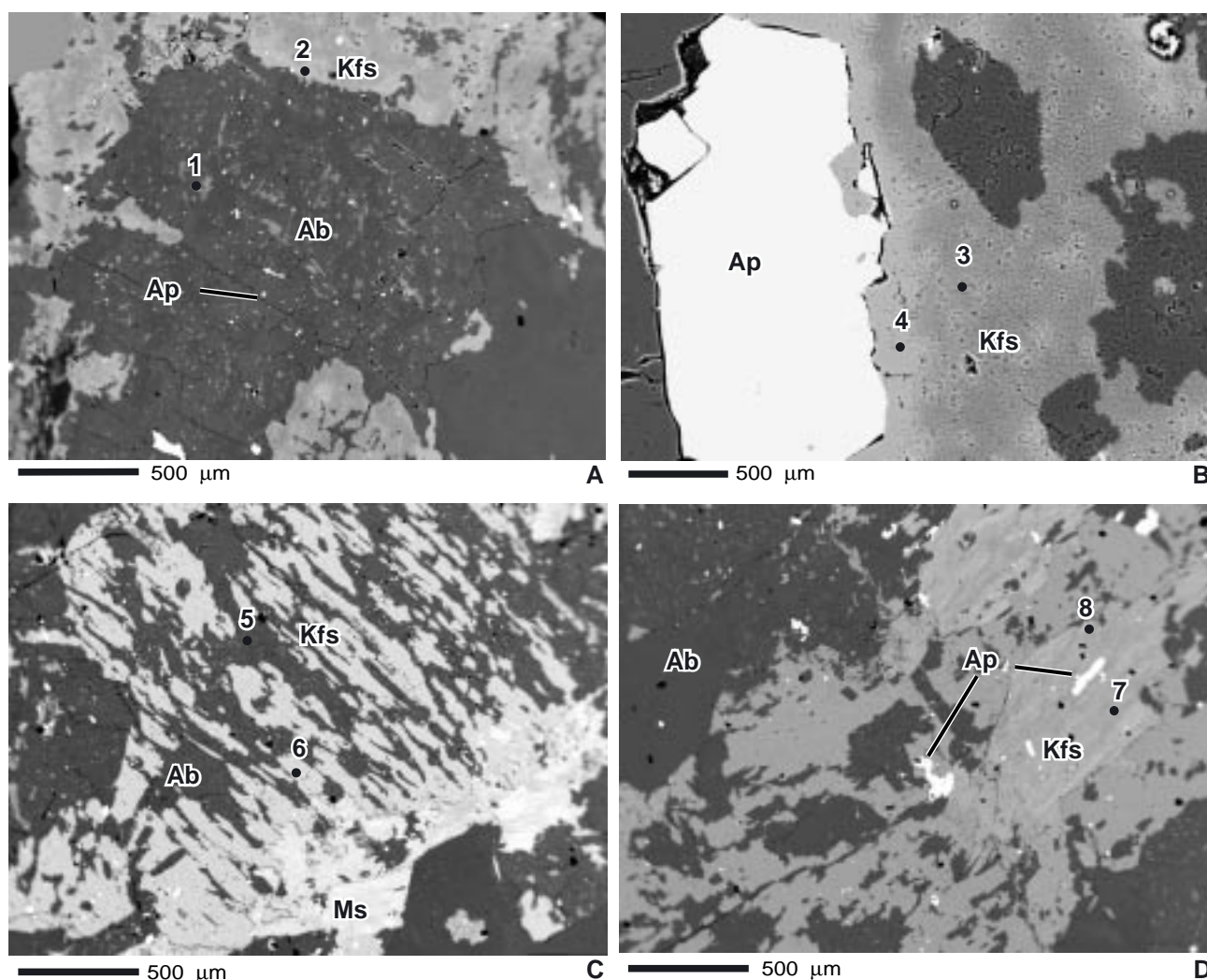
Fig. 3. BSE images of feldspar from the coarse-grained and fine-grained granites. Numbers indicate the analysis positions which are presented in Table 1. A, B – GK-8; C, D – GK-9. The numerous small bright spots in the albite (Ab) grains (Fig 1A, D) are from tiny secondary apatite crystals.

employed. For the determination of low levels of P in feldspar, a 60 sec count time was used and measured on the P Kα line utilising a high reflectivity PET crystal. Apatite was analysed using a Cameca SX50 electron microprobe at the Natural History Museum, London. Operating conditions were 15 kV, 25 nA beam current and, depending on the apatite grain size, a 1–5 μm diameter beam.

### Results

Petrological and mineralogical description

The samples studied of the principal granitic rocks from the Hnilec profile showed variable degrees of visible mineralization. The Hnilec two-mica granite from the lowermost part is a medium-grained rock consisting of hypidiomorphic, sericitized plagioclase (31 vol%), perthitic K-feldspar (24 vol%), quartz (37 vol%), muscovite (5 vol%), and minor biotite (1 vol%). The main accessory minerals are tourmaline, zircon, apatite, monazite, xeno-

time, rutile and fluorite. The upper emplaced medium-grained Ms granite consists of plagioclase (33 vol%), K-feldspar (25 vol%), quartz (34 vol%) and muscovite (8 vol%). Accessory minerals are represented mainly by tourmaline, zircon, apatite, monazite, xenotime, fluorite and rare cassiterite and Nb,Ta-minerals. The fine-grained granite has the lowest amount of feldspar, and highest quartz, comprising plagioclase (26.7 vol%), K-feldspar (12.5 vol%), quartz (44.7 vol%) and muscovite (16.6 vol%). Zircon, uraninite, monazite, garnet and Nb,Ta-minerals are the principal accessory minerals. The greisen consists of quartz (60 vol%) and muscovite (38 vol%), and locally, relicts of plagioclase could be identified. In the greisen, clusters of tourmaline, relatively abundant cassiterite and increased amounts of topaz, fluorite, arsenopyrite, molybdenite and pyrite are typical.

Compositions of some of the rock forming minerals

The feldspar compositions show some specific features relating to the P contents both in the albite and K-feldspar

Igor Broska – Michal Kubiš – C. Terry Williams – Patrik Konečný

Table 1. Representative microprobe analyses (in wt% oxide) of feldspar.

| Pos | 1 | 2 | 3 | 4 | 5 | 6 | 7 | 8 |
|---|---|---|---|---|---|---|---|---|
| Min | Ab | Kfs | Kfs | Kfs | Ab | Kfs | Ab | Kfs |
| Sample | GK-8/5-2 | GK-8/5-6 | GK-8/4-3 | GK-8/4-4 | GK-9/1-3 | GK-9/4-1 | GK-9/4-2 | GK-9/4-3 |
| $SiO_2$ | 69.36 | 64.90 | 61.21 | 65.01 | 69.44 | 65.29 | 65.18 | 65.62 |
| $Al_2O_3$ | 19.41 | 18.27 | 21.53 | 18.06 | 19.41 | 18.23 | 18.33 | 18.27 |
| FeO | 0.00 | 0.01 | 0.01 | 0.05 | 0.01 | 0.00 | 0.00 | 0.00 |
| CaO | 0.02 | 0.00 | 0.09 | 0.17 | 0.06 | 0.00 | 0.00 | 0.00 |
| $Na_2O$ | 11.74 | 0.28 | 0.29 | 0.19 | 11.53 | 0.24 | 0.28 | 0.22 |
| $K_2O$ | 0.10 | 16.30 | 15.40 | 16.42 | 0.08 | 16.58 | 16.69 | 16.73 |
| $P_2O_5$ | 0.02 | 0.04 | 0.00 | 0.00 | 0.05 | 0.11 | 0.00 | 0.00 |
| TOTAL | 100.64 | 99.80 | 98.53 | 99.90 | 100.57 | 100.44 | 100.48 | 100.84 |
| calculated on the basis 8 O | | | | | | | | |
| $Si^{4+}$ | 3.007 | 3.004 | 2.869 | 3.009 | 3.009 | 3.005 | 3.002 | 3.010 |
| $Al^{3+}$ | 0.992 | 0.996 | 1.189 | 0.985 | 0.992 | 0.989 | 0.995 | 0.987 |
| $Fe^{2+}$ | 0.000 | 0.000 | 0.000 | 0.002 | 0.000 | 0.000 | 0.000 | 0.000 |
| $Ca^{2+}$ | 0.001 | 0.000 | 0.005 | 0.008 | 0.003 | 0.000 | 0.000 | 0.000 |
| $Na^+$ | 0.987 | 0.025 | 0.027 | 0.017 | 0.969 | 0.021 | 0.025 | 0.020 |
| $K^+$ | 0.005 | 0.963 | 0.921 | 0.970 | 0.004 | 0.973 | 0.981 | 0.979 |
| $P^{5+}$ | 0.001 | 0.002 | 0.000 | 0.000 | 0.002 | 0.004 | 0.000 | 0.000 |
| $X_{Ab}$ | 0.994 | 0.026 | 0.028 | 0.017 | 0.993 | 0.021 | 0.025 | 0.020 |
| $X_{An}$ | 0.001 | 0.000 | 0.005 | 0.008 | 0.003 | 0.000 | 0.000 | 0.000 |
| $X_{Or}$ | 0.005 | 0.974 | 0.967 | 0.974 | 0.004 | 0.979 | 0.975 | 0.980 |

Table 2. Representative microprobe analyses (in wt% oxide) of white mica.

| No | 1 | 2 | 3 | 4 | 5 | 6 |
|---|---|---|---|---|---|---|
| Sample | GK-8 | GK-8 | GK-9 | GK-9 | GK-10 | GK-10 |
| $SiO_2$ | 46.60 | 47.16 | 48.37 | 47.09 | 48.23 | 46.98 |
| $TiO_2$ | 0.35 | 0.14 | 0.14 | 0.08 | 0.16 | 0.00 |
| $Al_2O_3$ | 32.78 | 31.70 | 28.12 | 30.12 | 30.62 | 34.19 |
| $Cr_2O_3$ | 0.00 | 0.01 | 0.05 | 0.15 | 0.00 | 0.04 |
| FeO | 3.89 | 3.04 | 6.53 | 5.78 | 5.64 | 3.86 |
| MnO | 0.11 | 0.07 | 0.23 | 0.21 | 0.02 | 0.06 |
| MgO | 0.34 | 1.71 | 0.24 | 0.06 | 0.41 | 0.02 |
| CaO | 0.00 | 0.04 | 0.00 | 0.00 | 0.00 | 0.00 |
| $Na_2O$ | 0.46 | 0.16 | 0.07 | 0.20 | 0.13 | 0.21 |
| $K_2O$ | 9.62 | 10.29 | 10.92 | 10.80 | 10.03 | 10.76 |
| F | 0.00 | 0.44 | 1.87 | 2.26 | 0.70 | 0.53 |
| Cl | 0.01 | 0.00 | 0.01 | 0.01 | 0.00 | 0.00 |
| total | 94.16 | 94.76 | 96.55 | 96.76 | 96.79 | 96.56 |
| O=F, Cl | 0.00 | 0.19 | 0.79 | 0.95 | 0.29 | 0.23 |
| TOTAL | 94.16 | 94.58 | 95.76 | 95.81 | 96.50 | 96.34 |
| calculated on the basis 22 O | | | | | | |
| Si | 6.325 | 6.386 | 6.664 | 6.487 | 6.501 | 6.267 |
| Ti | 0.036 | 0.014 | 0.015 | 0.008 | 0.016 | 0.000 |
| $Al^{IV}$ | 1.675 | 1.614 | 1.336 | 1.513 | 1.499 | 1.733 |
| $Al^{VI}$ | 3.568 | 3.445 | 3.231 | 3.377 | 3.365 | 3.654 |
| Cr | 0.000 | 0.000 | 0.000 | 0.000 | 0.000 | 0.000 |
| Fe | 0.442 | 0.344 | 0.752 | 0.666 | 0.636 | 0.432 |
| Mn | 0.010 | 0.007 | 0.022 | 0.020 | 0.002 | 0.006 |
| Mg | 0.069 | 0.345 | 0.049 | 0.012 | 0.083 | 0.004 |
| Ca | 0.000 | 0.006 | 0.000 | 0.000 | 0.000 | 0.000 |
| Na | 0.121 | 0.042 | 0.019 | 0.053 | 0.021 | 0.054 |
| K | 1.666 | 1.778 | 1.919 | 1.898 | 1.893 | 1.835 |
| F | 0.000 | 0.185 | 0.785 | 0.949 | 0.181 | 0.223 |
| Cl | 0.002 | 0.000 | 0.002 | 0.002 | 0.000 | 0.002 |

(0.0x wt%, Table 1 anal. No. 2, and Fig. 3A, B. However, K-feldspars from the apical fine-grained granites, i.e. those rocks that are more evolved, are more enriched in P with $P_2O_5$ contents up to 0.10 wt% (Table 1 anal. No. 6, Fig. 3C). It should be noted however, that some individual K-feldspar crystals contain exsolved apatite grains, similar to K-feldspar from the adjacent coarse-grained granites, are also free of P (Table 1 anal. No. 7, 8, Fig. 3D). Albite from this coarse-grained granite has very low contents of P (<0.0x wt%), although albite, exsolved from the K-feldspar as perthitic phase, can occasionally reach $P_2O_5$ contents of 0.05 wt% (Table 1 anal. No. 5).

X-ray diffraction and microprobe data indicate that the white mica present in the coarse-grained, fine-grained and greisenized granites is muscovite, and it is present as both a primary and secondary generation mineral. The secondary muscovite develops in feldspar crystals, whereas the primary muscovite is distributed mainly in interstitial localities. The muscovite contains relatively high concentrations of Fe, but is heterogeneously distributed. Within one grain, the $FeO_{tot}$ content varies from 2 wt% to 9 wt% and so this "phengitic component" is not simply a reflection of the Alpine metamorphic overprint of these granites. The F content in muscovite, including muscovite from the greisenized granite, is generally very low, although some F enrichment was detected in the fine-grained granites. The white mica corresponds to ferro-aluminoceladonite (Rieder et al. 1998) (Table 2).

within the principal granitic rocks of the Hnilec-Medvedí potok locality. The P concentrations vary in the alkali feldspars, although some general features are apparent. In all cases, albite contains very low (or below detection) concentrations of P (e.g. Table 1 anal. No. 1, Fig. 3A). The K-feldspars in the deepest coarse-grained leucogranite (see profile) usually contain very low concentrations of $P_2O_5$

Accessory apatite

The alkali feldspars in the Hnilec granitic rocks are characterized by the presence of newly-formed apatite crystals that are located mainly in albite. These apatite crystals are usually very small, typically less than 3 microns in size (Fig. 3A, D). They are considered to be late
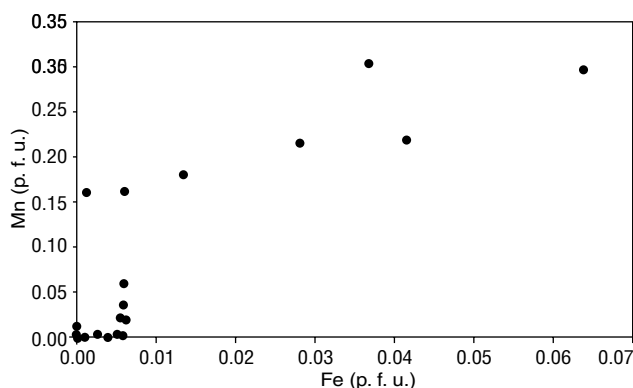
Fig. 4. Fe vs Mn binary plot of apatite from the Hnilec granites (samples GK-8, GK-9, GZ-1, GZ-3).
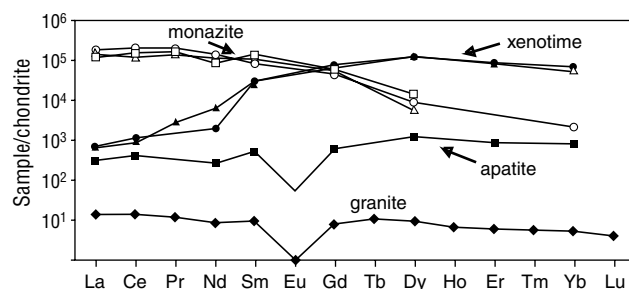


Fig. 5. Chondrite-normalized REE patterns of minerals from the coarse-grained Hnilec granite. The whole rock REE pattern, plotted for comparison, is the average of 3 coarse-grained Hnilec granite samples. The apatite pattern is the average of all primary apatite compositions from the studied area.

Note the large range in REE abundances among these minerals, particularly the high concentration in monazite (LREE) and xenotime (HREE), and the low but similar concentration and pattern of apatite compared with the bulk rock.

Table 3. Representative microprobe analyses (in wt% oxide) of apatites. Primary apatite are those from grains >50 μm in size; secondary apatite are those ~5 μm in size, and distributed within albite crystals.

| | sample GK-8 | | | | |
|---|---|---|---|---|---|
| type | primary (?) | primary (?) | primary (?) | secondary | secondary |
| grain | 1 | 2 | 3 | 4 | 5 |
| $SO_3$ | 0.00 | 0.03 | 0.08 | 0.00 | 0.00 |
| $P_2O_5$ | 41.61 | 41.61 | 42.34 | 41.91 | 42.10 |
| $SiO_2$ | 0.00 | 0.04 | 0.05 | 0.34 | 0.07 |
| $ThO_2$ | 0.03 | 0.03 | 0.06 | 0.01 | 0.06 |
| $UO_2$ | 0.01 | 0.10 | 0.14 | 0.09 | 0.00 |
| $La_2O_3$ | 0.00 | 0.01 | 0.03 | 0.00 | 0.00 |
| $Ce_2O_3$ | 0.04 | 0.03 | 0.02 | 0.05 | 0.19 |
| $Pr_2O_3$ | 0.05 | 0.08 | 0.00 | 0.21 | 0.03 |
| $Nd_2O_3$ | 0.07 | 0.05 | 0.00 | 0.09 | 0.05 |
| $Sm_2O_3$ | 0.02 | 0.03 | 0.02 | 0.01 | 0.06 |
| $Gd_2O_3$ | 0.01 | 0.02 | 0.00 | 0.06 | 0.00 |
| $Dy_2O_3$ | 0.00 | 0.01 | 0.00 | 0.00 | 0.04 |
| $Y_2O_3$ | 0.07 | 0.03 | 0.07 | 0.00 | 0.07 |
| $Al_2O_3$ | 0.00 | 0.03 | 0.05 | 0.09 | 0.03 |
| CaO | 52.42 | 51.03 | 53.13 | 54.16 | 55.27 |
| SrO | 0.02 | 0.03 | 0.13 | 0.00 | 0.01 |
| FeO | 0.40 | 0.91 | 0.19 | 0.06 | 0.00 |
| MnO | 3.04 | 4.16 | 2.54 | 0.32 | 0.03 |
| MgO | 0.00 | 0.00 | 0.01 | 0.02 | 0.00 |
| $Na_2O$ | 0.07 | 0.01 | 0.01 | 0.06 | 0.04 |
| F | 3.65 | 2.92 | 2.38 | 3.06 | 3.20 |
| Cl | 0.08 | 0.04 | 0.00 | 0.04 | 0.00 |
| OH | 0.02 | 0.32 | 0.34 | 0.28 | 0.34 |
| total | 101.61 | 101.51 | 101.58 | 101.40 | 101.61 |
| O=F, Cl | 1.55 | 1.24 | 1.00 | 1.30 | 1.35 |
| TOTAL | 100.06 | 100.27 | 100.58 | 99.54 | 100.26 |
| S | 0.000 | 0.002 | 0.006 | 0.000 | 0.000 |
| P | 2.990 | 3.011 | 3.040 | 3.003 | 3.011 |
| Si | 0.000 | 0.004 | 0.004 | 0.029 | 0.006 |
| Th | 0.001 | 0.001 | 0.001 | 0.000 | 0.001 |
| U | 0.000 | 0.002 | 0.003 | 0.002 | 0.000 |
| La | 0.000 | 0.000 | 0.001 | 0.000 | 0.000 |
| Ce | 0.001 | 0.001 | 0.000 | 0.001 | 0.006 |
| Pr | 0.002 | 0.002 | 0.000 | 0.006 | 0.001 |
| Nd | 0.002 | 0.002 | 0.000 | 0.003 | 0.002 |
| Sm | 0.001 | 0.001 | 0.001 | 0.000 | 0.002 |
| Gd | 0.000 | 0.001 | 0.000 | 0.002 | 0.000 |
| Dy | 0.000 | 0.000 | 0.000 | 0.000 | 0.001 |
| Y | 0.003 | 0.002 | 0.003 | 0.000 | 0.003 |
| Al | 0.000 | 0.003 | 0.004 | 0.009 | 0.002 |
| Ca | 4.768 | 4.672 | 4.828 | 4.912 | 5.001 |
| Sr | 0.001 | 0.002 | 0.006 | 0.000 | 0.001 |
| Fe | 0.029 | 0.065 | 0.014 | 0.004 | 0.000 |
| Mn | 0.219 | 0.301 | 0.182 | 0.023 | 0.002 |
| Mg | 0.000 | 0.000 | 0.001 | 0.002 | 0.000 |
| Na | 0.011 | 0.001 | 0.002 | 0.009 | 0.007 |
| XApFAp | 0.978 | 0.788 | 0.637 | 0.820 | 0.854 |
| XApClAp | 0.011 | 0.006 | 0.000 | 0.005 | 0.000 |
| XApHAp | 0.010 | 0.206 | 0.363 | 0.175 | 0.145 |

magmatic or secondary phases. In contrast, exsolved apatites distributed within K-feldspar crystals, form much larger grains (generally >250 microns in size), and often with xenomorphic (irregular) shapes, but can also occur as idiomorphic forms (Fig. 3D). The newly-formed apatite had the effect of decreasing the P contents in both orthoclase and plagioclase feldspar, but the presence of minor Ca in the Na-feldspar provides more suitable conditions for apatite formation and consequently it is more common in albite (Fig. 3A, Table 1). The crystallisation of secondary apatite was enhanced by the high F activity in the late-stage corrosive fluid. The formation of pure end-member albite and muscovite accompanied this late-stage process.

Apatite from the Hnilec granites forms two genetic types, illustrated by the Mn *vs.* Fe binary plot (Fig. 4). The first type is represented by the large exsolved apatite crystals distributed within the K-feldspar (e.g. Fig. 3B) and displays a positive correlation between Mn and Fe. Additionally, this apatite type has significantly higher Mn and Fe contents than the second genetic type - the small, newly-formed crystals in albite (e.g. Fig. 3A). This secondary apatite, distributed in Na-feldspar, is closest to stoichio-metric apatite as it contains the lowest contents of Mn and Fe, and is also depleted in REE. In contrast, the Mn-rich apatite (Fig. 4, Table 3) is similar to apatite from "classical" S-type granites (Sha and Chappell 2000; Broska et al. in prep.).

151

Table 4. Representative microprobe analyses (in wt% oxide) of monazite and xenotime from the coarse-grained granite

| | | | | Sample GK-8 | | | | |
|---|---|---|---|---|---|---|---|---|
| Point | 14.1 | 15.1 | 15.2 | 15.21 | 17.1 | 18.1 | 13.1 | 13.2 |
| Min | Mnz | Mnz | Mnz | Mnz | Xen | Xen | Xen | Xen |
| $P_2O_5$ | 29.17 | 28.04 | 28.01 | 28.57 | 32.66 | 32.84 | 31.85 | 31.21 |
| $SiO_2$ | 0.55 | 0.94 | 1.27 | 0.77 | 0.74 | 0.89 | 0.66 | 0.84 |
| $ThO_2$ | 4.57 | 10.87 | 11.26 | 9.54 | 0.56 | 0.65 | 1.32 | 1.07 |
| $UO_2$ | 0.09 | 0.15 | 0.25 | 0.00 | 2.62 | 1.23 | 2.29 | 3.49 |
| $La_2O_3$ | 11.03 | 7.476 | 7.88 | 7.46 | 0.00 | 0.04 | 0.00 | 0.00 |
| $Ce_2O_3$ | 30.08 | 24.02 | 25.55 | 25.24 | 0.15 | 0.17 | 0.28 | 0.00 |
| $Pr_2O_3$ | 3.99 | 3.22 | 3.32 | 3.38 | 0.06 | 0.00 | 0.02 | 0.06 |
| $Nd_2O_3$ | 13.28 | 13.17 | 11.25 | 13.05 | 0.70 | 0.21 | 0.61 | 0.66 |
| $Sm_2O_3$ | 3.12 | 4.44 | 4.29 | 4.72 | 0.94 | 1.08 | 1.16 | 0.91 |
| $Gd_2O_3$ | 1.97 | 2.88 | 2.51 | 2.68 | 3.00 | 3.17 | 3.32 | 3.07 |
| $Dy_2O_3$ | 0.48 | 0.80 | 0.63 | 0.33 | 6.85 | 6.83 | 6.58 | 6.28 |
| $Er_2O_3$ | n.d. | n.d. | n.d. | n.d. | 2.83 | 2.97 | n.d. | n.d. |
| $Yb_2O_3$ | 0.07 | 0.00 | 0.00 | 0.00 | 1.84 | 2.27 | 2.17 | 2.12 |
| $Y_2O_3$ | 0.49 | 1.28 | 0.83 | 0.58 | 42.19 | 41.50 | 41.38 | 40.45 |
| $Al_2O_3$ | 0.09 | 0.04 | 0.02 | 0.03 | 0.00 | 0.00 | 0.00 | 0.00 |
| $CaO$ | 0.52 | 1.68 | 1.64 | 1.64 | 0.13 | 0.14 | 0.20 | 0.17 |
| $MnO$ | 0.14 | 0.01 | 0.00 | 0.12 | 0.08 | 0.00 | 0.00 | 0.01 |
| $SrO$ | 0.00 | 0.04 | 0.00 | 0.19 | 0.00 | 0.00 | 0.00 | 0.00 |
| $PbO$ | 0.01 | 0.14 | 0.21 | 0.00 | 0.37 | 0.22 | 0.45 | 0.41 |
| Total | 99.65 | 99.18 | 98.92 | 98.31 | 95.73 | 94.21 | 92.30 | 90.76 |
| | | | | calculated on the basis 4 O | | | | |
| P | 0.978 | 0.954 | 0.953 | 0.972 | 0.970 | 0.979 | 0.975 | 0.972 |
| Si | 0.022 | 0.038 | 0.051 | 0.031 | 0.026 | 0.031 | 0.024 | 0.031 |
| Th | 0.041 | 0.099 | 0.103 | 0.087 | 0.004 | 0.005 | 0.011 | 0.009 |
| U | 0.001 | 0.001 | 0.002 | 0.000 | 0.020 | 0.010 | 0.018 | 0.029 |
| La | 0.161 | 0.111 | 0.117 | 0.111 | 0.000 | 0.001 | 0.000 | 0.000 |
| Ce | 0.436 | 0.353 | 0.376 | 0.371 | 0.002 | 0.002 | 0.004 | 0.000 |
| Pr | 0.058 | 0.047 | 0.049 | 0.049 | 0.001 | 0.000 | 0.000 | 0.001 |
| Nd | 0.188 | 0.189 | 0.161 | 0.187 | 0.009 | 0.003 | 0.008 | 0.009 |
| Sm | 0.043 | 0.061 | 0.059 | 0.065 | 0.011 | 0.013 | 0.014 | 0.012 |
| Gd | 0.026 | 0.038 | 0.033 | 0.036 | 0.035 | 0.037 | 0.040 | 0.037 |
| Dy | 0.006 | 0.010 | 0.008 | 0.004 | 0.077 | 0.077 | 0.077 | 0.074 |
| Er | n.d. | n.d. | n.d. | n.d. | 0.033 | 0.035 | n.d. | n.d. |
| Yb | 0.001 | 0.000 | 0.000 | 0.000 | 0.020 | 0.024 | 0.024 | 0.024 |
| Y | 0.010 | 0.027 | 0.018 | 0.012 | 0.787 | 0.777 | 0.796 | 0.792 |
| Al | 0.010 | 0.004 | 0.002 | 0.003 | 0.000 | 0.000 | 0.000 | 0.000 |
| Ca | 0.022 | 0.072 | 0.071 | 0.071 | 0.005 | 0.005 | 0.008 | 0.007 |
| Mn | 0.004 | 0.000 | 0.000 | 0.003 | 0.002 | 0.000 | 0.000 | 0.000 |
| Sr | 0.000 | 0.001 | 0.000 | 0.005 | 0.000 | 0.000 | 0.000 | 0.000 |
| Pb | 0.000 | 0.002 | 0.002 | 0.000 | 0.004 | 0.002 | 0.004 | 0.004 |
| Mo | 93.63 | 83.00 | 82.45 | 84.30 | – | – | – | – |
| Br | 4.21 | 13.28 | 12.45 | 12.63 | – | – | – | – |
| Hu | 2.16 | 3.72 | 5.11 | 3.08 | – | – | – | – |

The REE distribution of the primary apatite broadly reflects the bulk REE distribution of the host granitic rock (Fig. 5), as apatite is the principal phase hosting the REE. There are minor contributions from monazite (LREE) and from xenotime (HREE) (Table 4, Fig. 5), particularly in those granites with very low La/Yb ratios ($\approx 4$). Zircon also contributes to the HREE budget of the whole rock.

Accessory zircon

The morphologies of zircon crystals from all the investigated granites in the Hnilec vertical profile have very similar typological features. There are dominated by low S and L zircon types with the mean point represented by the $S_8$ typological subtype (Fig. 6). The same morphological type is present in both the coarse- and fine-grained granites, as well as in the greisen or strongly greisenized granite types. This similarity of zircon morphology from the different Spiš-Gemer granitic rocks suggests that this largest population of zircons originated from a common magma source, probably as an early crystallized phase transported by residual melts to their final emplacement in the granitic rocks. It is likely that only zircons with $G_1$ and some L subtypes were formed in the already emplaced granites (Fig. 7).

The CL images of zircon show a distinctive oscillatory zonation for all of the investigated crystals. Oscillatory zoning is a common feature in zircons from acid igneous rocks and is believed to have formed during long periods of crystallization. This feature supports the hypothesis that the majority of zircons from the Hnilec granites crystallized in the deep-seated magma chambers (Fig. 8A, B), and is further supported by the presence of two zircon nuclei centres present in one grain (Fig. 8A).

The zircon nuclei display magmatic oscillatory zonation, and have rounded forms indicating a complex crystallization/resorption process had taken place over a long period of time. After some significant change in the magma composition, the relative growth rates of different zircon crystal faces changed, preferentially favouring the growth of pyramidal (311) planes (Vavra 1990). It seems likely that such a complex crystal growth history could only be achieved from the zircon residing for long periods of time in different magma batches. The oscillatory zoning of zircons is locally overprinted, probably by changes in fluid composition and perhaps by loss of U, Th, Pb, that accompanied this process (Pidgeon 1992).

Microprobe analyses of zircon showed that P was below the detection limit, and that the Zr/Hf ratios were relatively constant around a mean value of ~31 (Table 5), which is typical for magmatic zircons from anatectic rocks (Pupin, 2000). Some variation in Y (and U) was observed, with Y showing some degree of correlation with Hf. As P was not present in the zircon, no epitaxial xenotime overgrowths were observed and xenotime crystallized as a separate phase (Fig. 7).
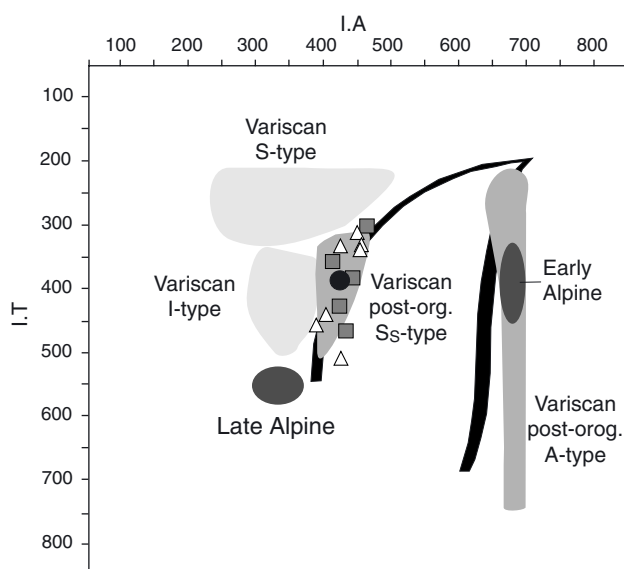
Fig. 6. The projection of the typological mean points of zircons from granites in the Spiš-Gemer area. Zircon typological mean points from the Hnilec region are represented by squares; those from Betliar, Poproč and Hummell granite bodies are represented by triangles. Full circle show the position of the mean point of all samples. For comparison, fields for the Variscan I and S zircon mean points, and from the post-orogenic A-type granites are shown. Typogram and calculation of the mean points after Pupin (1980). The mean points of the investigated samples have the following parameters: GK-8: IA = 475, IT = 287 (where - IA = agpacity index, IT = index of temperature); GK-9: IA = 445, IT = 360; GK-10: IA = 423, IT = 330.
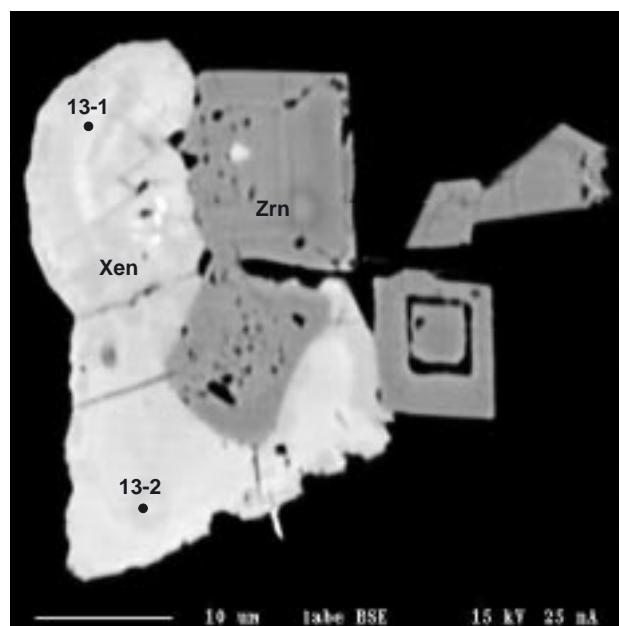


Fig. 7. BSE image of xenotime-zircon paragenesis. The zircon crystal is here cut perpendicular to the the c-axis, and the typologically belongs to $G_1$ or L subtype, which represents the most recent zircon crystallisation phase. The zonation observed in the xenotime is mainly due to the variations in concentrations of U, with the lighter areas of xenotime being enriched in U.

## Discussion and concluding remarks

Compositional features of one of the rock-forming minerals (feldspar), coupled with morphological characteristics of an accessory phase (zircon) combine to provide strong evidence for a cogenetic relationship between the main granitic phases at the Hnilec-Medvedí potok locality. The presence of the P in alkali feldspars in the Hnilec granites is the direct result of the high peraluminosity of the melt (ACNK >1.2) when P behaves as an incompatible element. Phosphorus precipitates in late magmatic apatite as well as being incorporated as a minor component in alkali feldspar. The concentration of P in alkali feldspar increases from the medium- to fine-grained granites and corresponds to an increase in Al activity in the melt. High P contents in alkali feldspars have been reported from all the evolved peralu-

minous granites, including tin-bearing types (Frýda and Breiter, 1995; Breiter et al., 1997; Breiter et al., 1999, 2002; Breiter, 2001). This incorporation of P in feldspar,

Table 5. Representative microprobe analyses (in wt% oxide) of the zircon. Zr/Hf$_w$ calculated from atomic weights.

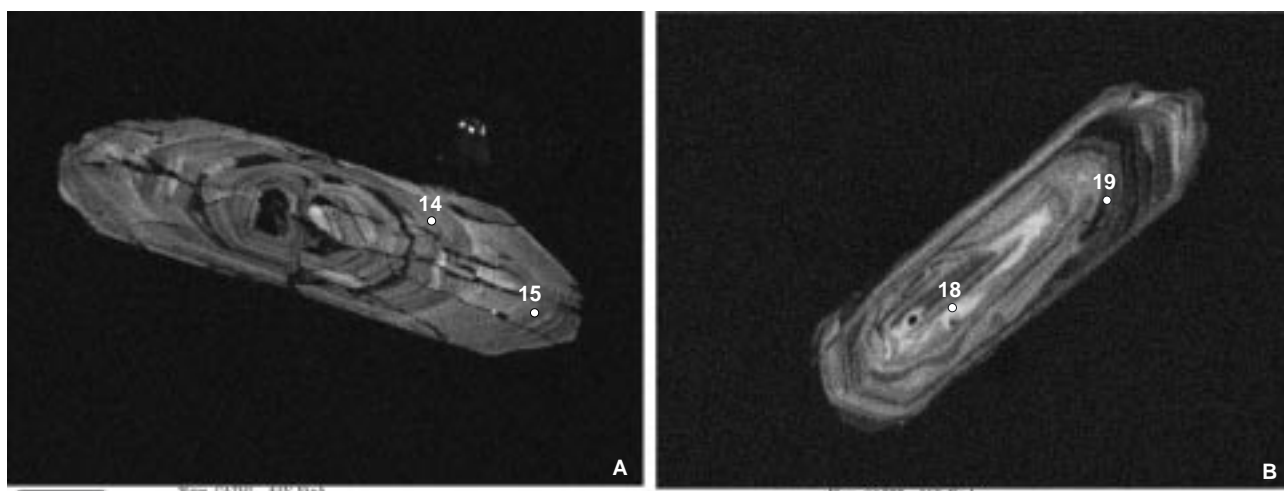| No. | 11 | 12 | 14 | 15 | 16 | 17 | 18 | 19 |
|---|---|---|---|---|---|---|---|---|
| Sample | GK-8 | GK-8 | GK-8 | GK-8 | GK-8 | GK-8 | GK-9 | GK-9 |
| grain | 1 | 1 | 2 | 2 | 3 | 3 | 1 | 1 |
| pos | core | rim | core | rim | core | rim | core | rim |
| SiO$_2$ | 32.52 | 32.52 | 33.38 | 33.81 | 32.28 | 32.47 | 33.02 | 30.05 |
| ZrO$_2$ | 65.47 | 65.47 | 63.71 | 63.41 | 64.33 | 63.38 | 63.48 | 64.31 |
| HfO$_2$ | 1.72 | 1.71 | 1.83 | 1.83 | 1.76 | 1.67 | 1.92 | 1.26 |
| ThO$_2$ | 0.01 | 0.02 | 0.01 | 0.00 | 0.03 | 0.00 | 0.05 | 0.10 |
| UO$_2$ | 0.02 | 0.08 | 0.05 | 0.00 | 0.00 | 0.14 | 0.02 | 0.05 |
| Al$_2$O$_3$ | 0.00 | 0.00 | 0.00 | 0.10 | 0.00 | 0.00 | 0.00 | 0.00 |
| Y$_2$O$_3$ | 0.00 | 0.08 | 0.03 | 0.07 | 0.34 | 0.52 | 0.19 | 0.44 |
| Yb$_2$O$_3$ | 0.09 | 0.00 | 0.04 | 0.08 | 0.13 | 0.19 | 0.11 | 0.04 |
| CaO | 0.00 | 0.01 | 0.00 | 0.04 | 0.00 | 0.00 | 0.00 | 0.00 |
| FeO | 0.00 | 0.07 | 0.02 | 0.00 | 0.00 | 0.10 | 0.04 | 0.00 |
| Total | 99.81 | 99.09 | 99.05 | 99.34 | 98.86 | 98.46 | 98.83 | 96.24 |
| calculated on the basis 4 O | | | | | | | | |
| Si$^{4+}$ | 1.001 | 1.022 | 1.027 | 1.034 | 1.004 | 1.012 | 1.021 | 0.970 |
| Zr$^{4+}$ | 0.983 | 0.960 | 0.956 | 0.946 | 0.975 | 0.963 | 0.958 | 1.012 |
| Hf$^{4+}$ | 0.015 | 0.016 | 0.016 | 0.016 | 0.016 | 0.015 | 0.017 | 0.012 |
| Th$^{4+}$ | 0.000 | 0.000 | 0.000 | 0.000 | 0.000 | 0.000 | 0.000 | 0.001 |
| U$^{4+}$ | 0.000 | 0.001 | 0.000 | 0.000 | 0.000 | 0.001 | 0.000 | 0.000 |
| Al$^{3+}$ | 0.000 | 0.000 | 0.000 | 0.003 | 0.000 | 0.000 | 0.000 | 0.000 |
| Y$^{3+}$ | 0.000 | 0.001 | 0.001 | 0.001 | 0.006 | 0.009 | 0.003 | 0.008 |
| Yb$^{3+}$ | 0.001 | 0.000 | 0.000 | 0.001 | 0.001 | 0.002 | 0.001 | 0.000 |
| Ca$^{2+}$ | 0.000 | 0.001 | 0.000 | 0.001 | 0.000 | 0.000 | 0.000 | 0.000 |
| Fe$^{2+}$ | 0.000 | 0.002 | 0.001 | 0.000 | 0.000 | 0.003 | 0.001 | 0.000 |
| Zr/Hf$_w$ | 33.4 | 30.5 | 30.4 | 30.3 | 31.9 | 33.0 | 28.8 | 44.5 |

Fig. 8. CL images of zircon crystals. Note the oscillatory zonation within the nucleus in image A. A – GK-8, B – GK-9.

known as the berlinite substitution, results from berlinite (ideally $AlPO_4$) being isostructural with the $Si_2O_4$ framework component of feldspar (London *et al.,* 1990; London, 1992; London, 1998). The influence of P on silicate melt structure is well known, and it has the effect of depolymerising melts that results in a lowering of the melt viscosity (Mysen *et al.,* 1981). The $M-PO_4$ complexes occur in the melt as a result of metal cation transfer from non-bridging oxygens (NBO) in the silicate portion of the melt structure, whereas the ratio of non-bridging oxygens to tetrahedral cation (NBO/T) is decreased. Coupled with an enrichment of volatile elements (such as $H_2O$, F, B) in the fluid phase, this decrease in the melt viscosity has the effect of mobilising and concentrating elements such as Sn, Nb and Ta in the cupolas of granite massifs, which locally show evidence for fluid-element saturation, indicated by minerals such as cassiterite, tourmaline and fluorite, together with albitization and greisenization. This process also operated in the cupola of the Hnilec granite body and resulted in an evolved tin mineralization stage. The cassiterite-bearing greisen forms part of the endocontact of the fine-grained granite intrusion as indicated by the composition and morphology of zircon being very similar to zircon from the main granitic phases.

The similarities of the granites from Hnilec-Medvedí potok locality and other granite bodies in the Hnilec area indicate a close genetic relationship to granite bodies in all of the Spiš-Gemer area. The zircon morphology in granites is very similar throughout the Spiš-Gemer region (Jakabská and Rozložník 1989, Broska and Uher 1991), and is undoubtedly a reflection of similar sources for, and similar evolution of, these granites. The zircon morphological and compositional characteristics have many features in common with zircons from aluminium-rich crustal granitoids (Jakabská and Rozložník 1989).

Evidence from zircon CL images and morphology suggest that the granites could be derived from batches of deep-seated granitic melt on the crust-mantle boundary formed by a heat source of the rift related mafic melt that occurred during the Permian-Triassic period. The high B concentration, so typical of the Spiš-Gemer granites, can be explained by an enrichment of their primary melts by B introduced from volcanic emanations that operated in the deep fault systems or rifts during the Permian period (Broska and Uher 2001), and particularly also from B-enriched mica sources (Petrík and Kohút 1997). The Spiš-Gemer granites in this sense may have resulted from melting triggered by increasing heat flow from the mantle below the continental crust, during the post-collisional extension of the Variscan orogeny. The rifting process that opened the Meliata-Hallstadt Ocean in the Triassic could have been a thermal source for melting of the Gemeric granites (Broska and Uher 2001) and what is evoked also by former assumed contact of the Gemeric terrain with the Meliata Ocean (Plašienka et al. 1999).

*R e f e r e n c e s*

Breiter K. (2001): Phosphorus- and fluorine-rich granite system at Podlesí. In: Breiter (ed.) Phosphorus- and fluorine-rich fractionated granites. Int. Workshop, Czech Geol. Surv., Prague, 52–78.

Breiter K., Förster H.-J., Seltmann R. (1999): Variscan silicic magmatism and related tin-tungsten mineralization in the Erzgebirge-Slavkovský les metallogenic province. Mineralium deposita, 34, 505–521.

Breiter J., Frýda J., Leichmann J. (2002): Phosphorus and rubidium in alkali feldspars: Case studies and possible genetic interpretation. Bull. Czech Geol. Surv. 77, 2, 93–104.

Breiter K., Frýda J., Seltmann R., Thomas R. (1997): Mineralogical evidence for two magmatic stages in the evolution of an extremely fractionated P-rich rare-metal granite: the Podlesí stock, Krušné hory, Czech Republic. J. Petrol., 38, 12, 1723–1739.

Broska I., Uher P. (1991): Regional typology of zircon and their rela-

tionship to allanite-monazite antagonism (on example of Hercynian granitoids of the Western Carpathians). Geologica Carpathica, 42, 271–277.

Broska I., Uher P. (2001): Whole-rock chemistry and genetic typology of the West-Carpathian granites. Geologica Carpathica, 52, 79–90.

Broska I., Uher P., Lipka J. (1998): Brown and blue schorl from the Spiš-Gemer granite, Slovakia: composition and genetic relations. Jour. Czech Geol. Soc., 43, 1, 9–16.

Broska I., Uher P., Siman P. (1999): Na sodík chudobný skoryl a foitit v spišsko-gemerských granitoch. Mineralia slovaca, 31, 507–512.

Cambel B., Kráľ J., Burchart J. (1990): Isotopic geochronology of the Western Carpathian crystalline complex with catalogue of data. Ve-da Publ., Bratislava, 1–183 (in Slovak with English summary).

Drnzík E. (1982): Factor controlling the tin mineralization in the Hnilec tin ore field. PhD thesis, Košice, 1–142 (in Slovak).

Faryad S., Dianiška I. (1989): Garnets from granitoids of the Spišsko-gemerské Rudohorie Mts. Geol. Zbor. Geol. carpath. 40, 715–734.

Finger F., Broska I. (1999): The gemeric S-type granites in southeastern Slovakia: Late Palaeozoic or Alpine intrusion? Evidence from the electron-microprobe dating of monazite. Schweiz. Mineral. Petrogr. Mitt., 79, 439–443.

Frýda J., Breiter K. (1995): Alkali feldspars as a main phosphorus reser-voirs in rare-metal granites: three examples from the Bohemian Mas-sif (Czech Republic). Terra Nova, 7, 315–320.

Grecula P. (ed.) (1985): Mineral deposits of the Slovak Ore Mountains vol. 1. Mineralia slovaca corporation, Bratislava, 1–829.

Jakabská K., Rozložník L. (1989): Zircons of gemeric granites (Western Carpathians – Czechoslovakia). Geol. Zbor. Geol. carpath., 40, 141–159.

London D. (1992): Phosphorus in S-type magmas: the $P_2O_5$ content of feldspars from peraluminious granites, pegmatites and rhyolites. American Mineralogist, 77, 126–145.

London D. (1998): Phosphorus-rich peraluminious granites. Acta Univer-sitatis Carolinae – Geologica, 42, 64–68.

London D., Černý P., Loomis J. L., Pan J. J. (1990): Phosphorus in alka-li feldspars of rare-element granitic pegmatites. Canadian Mineralo-gist, 28, 771–786.

Mysen B. O., Ryerson F. J., Virgo D. (1981): The structural of phospho-rus in silicate melts. American Mineralogist, 66, 106–117.

Petrík I., Kohút M. (1997): The evolution of granitoid magmatism during the Hercynian orogen in the Western Carpathians. In: Grecula et al. Geological evolution of the Western Carpathians. Mineralia slovaca Monograph, 235–252.

Plašienka D., Grecula P., Putiš M., Hovorka D., Kováč M. (1997): Evo-lution and and structure of the Western Carpathians: an overview. In: Grecula et al. (eds) Geological evolution of the Western Carpathians. Mineralia slovaca Monograph, 1–24.

Poller U., Uher P., Broska I., Janák M., Plašienka D. (2002): First Per-mian-Early Triassic zircon ages for tin-bearing granites from Ge-meric unit (Western Carpathians, Slovakia): connection to the post-collisional extension of the Variscan orogen and S-type mag-matism. Terra Nova, 14, 41–48.

Pupin J. P. (1980): Zircon and granite petrology. Contrib. Mineral. Petrol., 73, 207–220.

Pupin J. P. (2000): Granite genesis related to geodynamics from Hf-Y in zircon. Royal Trans. Soc. Edinburg, Earth Sciences, 91, 245–256.

Rieder M., Cavayyini G., Dyakonov Yu. S., Frank-Kamenetskii V. A., Gottardi G., Guggenheim S., Koval P. V., Mueller G., Neiva A. M. R., Radoslovich E. W., Robert J.-L., Sassi F. P., Takeda H., Weiss Y., Wones D. R. (1998): Nomenclature of the micas. Can. Mineralogist, 36, 905–912.

Rub M. G., Pavlov V. A., Cambel B., Veselský J. (1977): Typomorphic properties of biotite and accessory minerals in the Gemeric granites of Slovakia. Geol. Zbor. Geol. carpath., 28, 29–310 (in Russian).

Sha L. K., Chappell B. W. (2000): Apatite chemical composition, deter-mined by electron microprobe and laser-ablation inductively coupled plasma mass spectrometry, as a probe into granite petrogenesis. Geochim. Cosmochim. Acta, 63, 3861–3881.

Vavra G. (1990): On the kinematics of growth and its petrogenetic sig-nificance: a cathodoluminiscence study. Contrib. Mineral. Petrol., 90–99.

Vozárová A., Frank W., Kráľ J. (2000): [40]Ar/[39]Ar data from contact aure-ole of Súľová granite (Gemericum, the Western Carpathians). Slov. Geol. Magazine, 6, 363–366.